Hindawi
Geofluids
Volume 2020, Article ID 4543719, 8 pages
https://doi.org/10.1155/2020/4543719

Research Article

Shear Behavior and Anisotropy Characteristics of the Fracture Morphology of Sandstone with Different Water Contents

Changang Du,[1] **Lulu Sun**,[1,2,3] **Botao Qin**,[3] **Jiang Xu**,[4] **and Yixin Liu**[1,2]

[1]*School of Mining and Safety Engineering, Shandong University of Science and Technology, Qingdao 266590, China*
[2]*State Key Laboratory of Mining Disaster Prevention and Control Co-Founded by Shandong Province and the Ministry of Science and Technology, Shandong University of Science and Technology, Qingdao 266590, China*
[3]*School of Safety Engineering, China University of Mining and Technology, Xuzhou, Jiangsu 221116, China*
[4]*State Key Laboratory of Coal Mine Disaster Dynamics and Control, Chongqing University, Chongqing 400044, China*

Correspondence should be addressed to Lulu Sun; sun.sdust@sdust.edu.cn

Received 21 October 2019; Revised 7 January 2020; Accepted 3 February 2020; Published 12 February 2020

Academic Editor: Paola Gattinoni

Hydromechanical coupling in rock masses is an important issue for many rock mechanics and hydrogeology applications. The change of a water-bearing state will induce the fracture of the intact rocks and further accelerate the shear slip instability of the sheared surface. To investigate the weakening effect of water content on the mechanical properties of a rock mass, laboratory direct shear tests combined with three-dimensional analysis of sheared surfaces were carried out on sandstone samples with different water contents. The variogram parameters, sill and range, were applied to quantify the morphology of shear fracture surfaces, to reflect the shear failure process of the intact rock, and to provide a basis for resliding instability of jointed rock. It was determined that the sill represents the height of the fluctuation body in the fracture surface and the range represents the single fluctuation body and may reflect the frequency of fluctuations. The test results revealed that the increase in water content had a clear weakening effect on the shear strength and deformation behavior of rock, especially under saturated conditions. Moreover, the distribution of water in the samples directly affected the crack initiation and propagation and characteristics of the fracture morphology.

1. Introduction

Hydromechanical coupling in rock masses is an important issue for many rock mechanics and hydrogeology applications [1–7]. In mining and civil engineering, the redistribution of the stress field during the excavation of tunnels and underground caverns leads to the initiation and propagation of cracks, which can cause dramatic changes in the permeability of a rock mass [8, 9]. Hence, it is very important in engineering practice to study the failure and instability mechanisms of rock masses under the hydromechanical coupling action of groundwater [10]. Xiao et al. evaluated the equivalent porous media (EPM) and the relationship between force and deformation, and the flow rate of fluid through a fracture is especially critical [11]. Heiland and Raab reported that the permeability evolution of low-porosity sandstone is similar to that of crystalline rock under triaxial compression [12]. In the prefracture instability region, permeability decreases with compression stress and increases after expansion. When the volume of the specimen returns to the initial state, the permeability does not recover. Wang et al. reported that the pore pressure gradient field has an important influence on the propagation direction of the main tensile fracture [13]. Geertsma found that an increase in local pore water pressure can promote crack growth, while the overall increase in pore water pressure may inhibit the crack growth, especially for tensile cracks [14]. In the field of fluid injection research, it is considered that pore water pressure may induce fault slip and seismic events [15–17]. However, the hydromechanical coupling mechanisms still are poorly understood [18, 19].

It is worth noting that the effect of water content, which is the intermediate link of the rock mass changing from a dry state to a pore water pressure state, often has been neglected. It is well known that an increase in water content will reduce

Figure 1: Photograph of some sandstone samples.

the strength of a rock mass and will shorten the time before instability [20]. Meanwhile, the failure of rock is quite commonly induced by compressive and shear coupling loading [21–26]. Xu et al. reported that the tensile and shear damage of the weakest parts of a rock slope are the main factors that trigger failure of the rock slope [27]. Liu et al. developed a new mesoscopic shear apparatus and studied the crack propagation path and damage mechanisms under compression-shear loading [28, 29]. Thus, it is very meaningful to study the shear failure process of rocks with different water contents.

The aim of the present work was to study the shear instability process and secondary slip risk after shear failure, based on the evolution of water infiltration into the rock. Compression-shear tests of sandstone with different water contents were carried out. The effect of water content on the mechanical behavior and on the morphological characteristics of the sheared fracture surface was analyzed. To further assess the risk of continued slip instability after intact rock sheared, the variogram function was applied to quantify the anisotropy of postshearing 3D geometry of the fracture surface.

2. Experimental Procedure

2.1. Sample Preparation. The sandstone samples were obtained from the Three Gorges Reservoir, Chongqing, China. The samples were comprised primarily of quartz, feldspar, chert, and muscovite with a grain size distribution of 0.1 to 0.5 mm. Drilling cores without obvious fractures were selected and were cut into cubes with dimensions of approximately $100 \times 100 \times 100$ mm. Young's modulus of the samples was 6.79 GPa, the Poisson ratio was 0.26, the uniaxial compressive strength was 81.04 MPa, and the density was 2.32 g/cm^3. A picture of some of the sandstone samples is presented in Figure 1.

2.2. Test Design. The tests were divided into three groups, which were taken from the same intact rock block with the same normal stress and identical stress paths. Three water contents (0%, 50%, and 100%) were selected to be tested, and the detailed water content levels were determined in the following manner [30]:

(1) Firstly, a sample was dried in a drying oven at 105°C for 48 hours. It then was cooled to room temperature in a dry vessel. The water content (ω_w) of the sample then was considered to be 0%

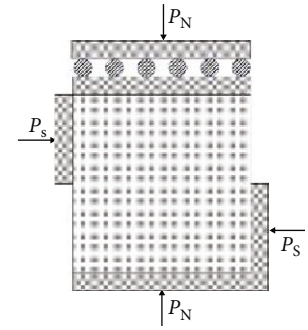

Figure 2: Force diagram of samples in a direct shear test.

(2) In the saturation process, a dry sample was immersed in a tank filled with purified water for 1 hour in a vacuum and then was weighed. The operation was repeated every hour until the weight of the sample remained unchanged. The sample was considered to be saturated ($\omega_w = 100\%$) in this study

(3) A saturated sample was placed in a laboratory with excellent ventilation. The sample was weighed every hour. The mass change values were used to calculate the water content according to

$$\omega_w = \frac{m_w - m_d}{m_d} \times 100\%, \quad (1)$$

where ω_w (%) is the water content of the specimen and m_w (g) and m_d (g) are the wet and dry masses of the sample, respectively.

Because of inaccuracy in these measurements, a water content value between 49% and 51% was assumed to be 50%. Figure 2 shows the loading status of the specimens. In the figure, P_N is a load to produce normal stress and P_S is a load to produce shear stress. The normal stress (P_N) that was applied to samples was considered 2 MPa. To digitize the morphology of the surface, the system projects a series of structured white light fringe patterns onto the surface of the object (see Figure 3). Two CCD cameras were employed to capture images of these patterns automatically. From these image pairs, high-density 3D point cloud data from the surface were calculated accurately [31]. Finally, digitized surface data were reconstructed at an interval of 0.2 mm.

3. Results

3.1. Shear Mechanical Behavior. In view of the consistent trend of the shear stress-shear strain curves under different conditions [30, 33], curves under saturated condition ($\omega_w = 100\%$) (Figure 4(a)) were analyzed. In the present study, a statistical comparison and analysis of the mechanical parameters were made at the peak shear stress under different conditions (Figures 4(b)–4(d)). It can be observed that as the shear strain increased during the initial stage, the shear stress and the normal strain increased in concavity form. This was due to the fact that the normal strain during the initial stage of loading was mainly associated with closure of the

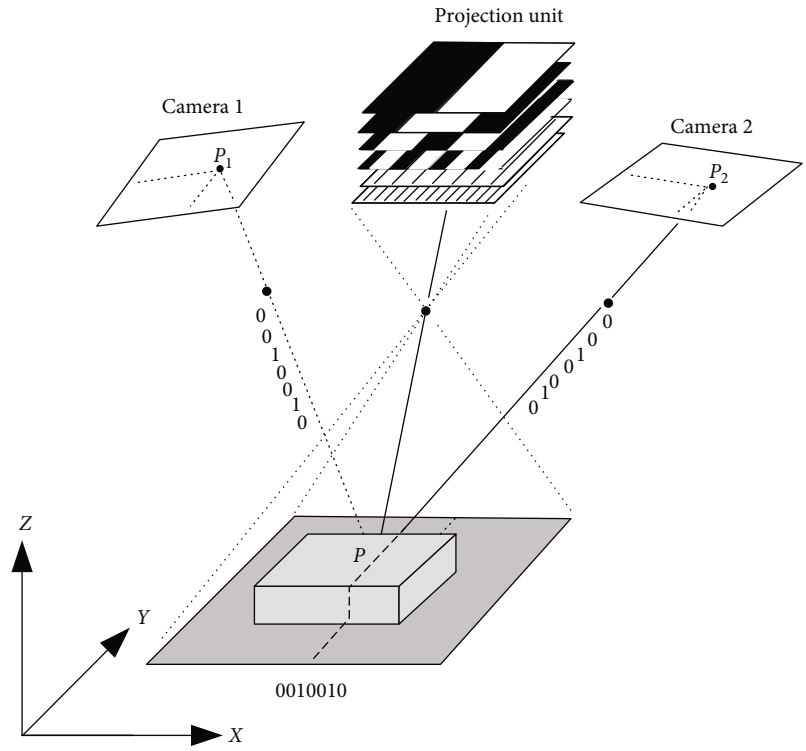

Figure 3: Principle of the advanced topometric sensor system [32].

microcracks, rather than to dilation resulting from microcracking and microfracture closure [34]. Then, the shear stress continued to rise after a period of fluctuation until shear failure occurred. With increasing water content, the mechanical parameters at the peak shear stress showed a decreasing trend (Figures 4(b)–4(d)). It should be concluded that the weakening effect of water on the mechanical properties of rock includes physical chemistry phenomena such as exfoliation, hydration, solution, oxidation, and abrasion [35] and mechanical action such as pore pressure [13]. When the water content reached 50%, the shear stress decreased by about 6%. However, when the water content reached 100%, the peak shear stress decreased by 20%. This indicated that the effect of mechanical action on shear strength was greater and the action of water physical chemistry just lowers the energy required for microcracking [36], whereas pore pressure reduces the effective stress. Under the condition where the sample was saturated with water, this resulted locally in the formation of pore water pressure in the sample and promoted the further initiation and expansion of microcracks, thus greatly reducing the peak shear stress because the seepage velocity of the water was low.

Meanwhile, peak shear strain increased when the water content reached 50% and decreased when the water content reached 100%. Peak normal strain decreased as the water content was increased. This further indicated that water softened the rock and pore pressure reduced the fracture toughness of tension cracks [13]. When the water content reached 100%, the tension cracks propagated further under the combined action of the local pore water pressure and weakening of the fracture toughness of the specimens without further expansion deformation which resulted in a significant decrease in the peak shear strain and peak normal strain.

This section may be divided into subheadings. It should provide a concise and precise description of the experimental results and their interpretation as well as the experimental conclusions that can be drawn.

3.2. Anisotropic Characteristics of the Shear Fracture Surface. The morphology of the fracture surface not only reflects the failure process [37] but also plays a dominant role in the mechanical and hydraulic behavior of discontinuous rock masses. The mechanical responses of a rock joint, such as its peak shear strength, are all dependent on the shear direction [38, 39]. Geostatistical methods are used to describe the anisotropy of joint surfaces because they are designed to characterize spatial variations [40]. In the present study, the variogram $\gamma(h,\theta)$ was employed to quantify the anisotropic characteristics of the shear fracture and was defined as

$$\gamma(h,\theta,) = \frac{1}{2N(h)} \sum_{i=1}^{N(h)} \{Z(x_i,y_i) - Z[(x_i,y_i) - h(\theta)]\}^2, \quad (2)$$

where $N(h)$ is the number of pairs of data whose lag is h, $Z(x_i,y_i)$ is the height at point (x_i,y_i), and $[Z(x_i,y_i) - h(\theta)]$ is the height at a radial distance h in a direction θ from (x_i,y_i).

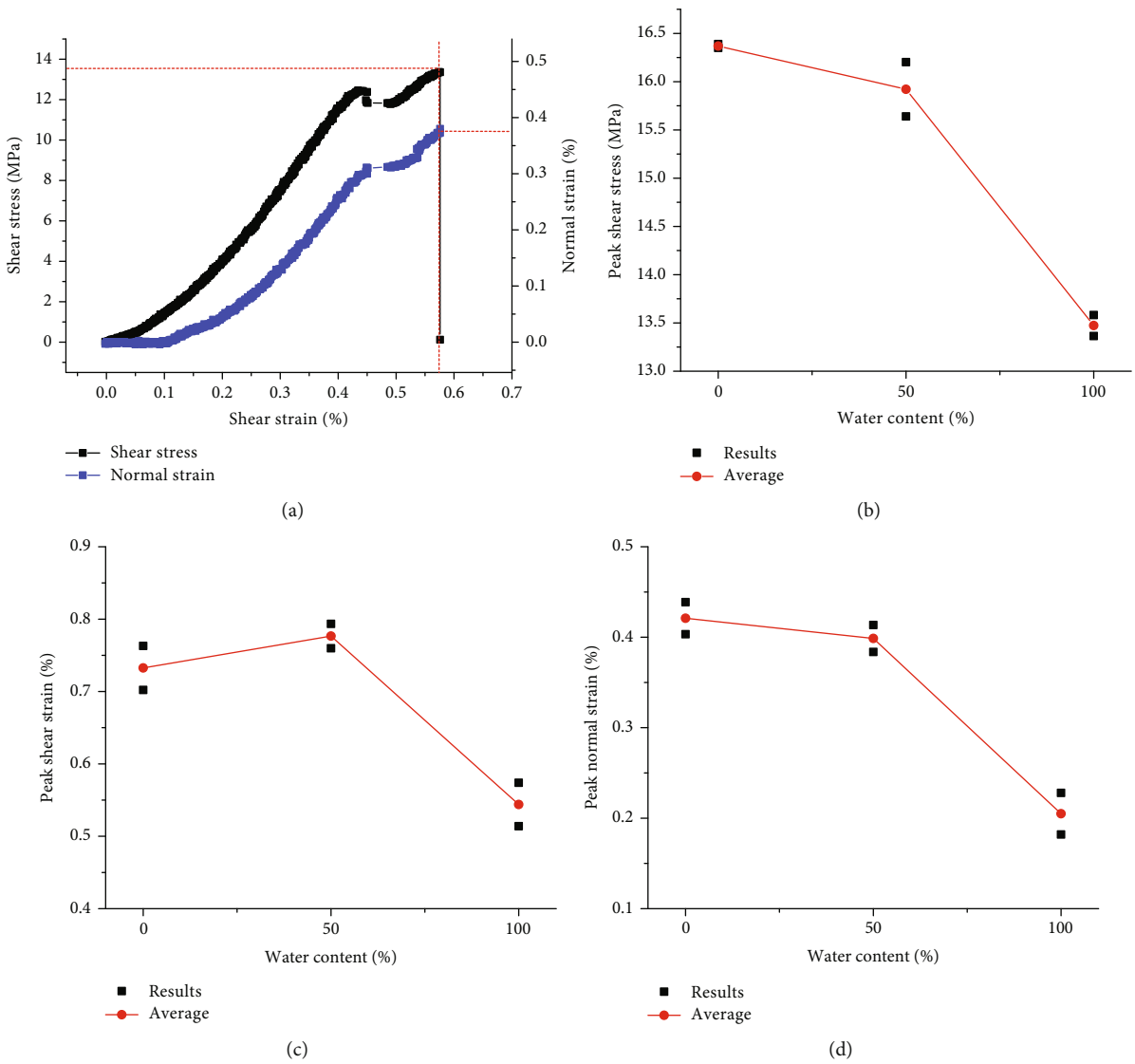

FIGURE 4: Variation curves of shear failure parameters under different water contents: (a) shear stress and normal strain vs. shear strain with $\omega_w = 100\%$, (b) peak shear stress, (c) peak shear strain, and (d) peak normal strain.

Here, a spherical model was used to fit the variogram function (Figure 5) and was defined to be

$$\gamma(h) = \begin{cases} 0, & h = 0, \\ C_0 + C\left(\frac{3}{2}\frac{h}{a} - \frac{1}{2}\left(\frac{h}{a}\right)^3\right), & 0 < h \le a, \\ C_0 + C, & h > a, \end{cases} \quad (3)$$

where C_0 is the nugget effect, C is the sill, a is the range, and h is the lag distance [41].

For the denser data, the nugget effect was zero [42]. The parameters of the variogram used in the present paper include the range and the sill.

The parameter distribution curve for the variogram at a water content of 100% is presented in Figure 6. It can be observed that the fracture surface is undulating along the

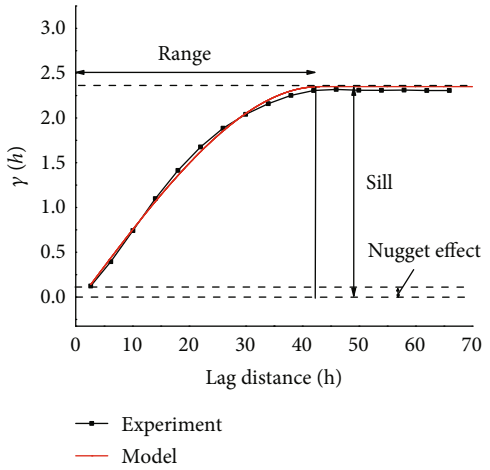

FIGURE 5: Variograms from the experimental tests and the best-fit spherical model for the fracture surface.

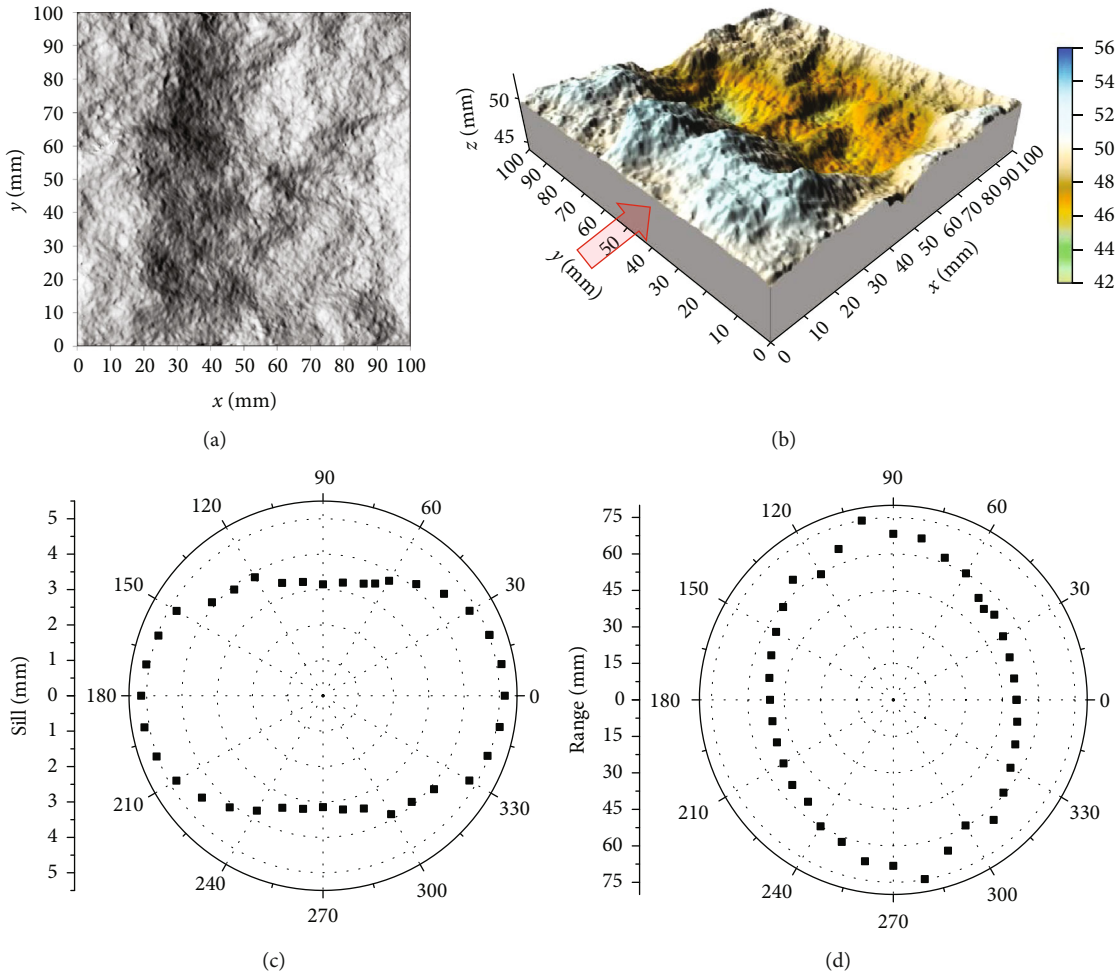

FIGURE 6: Parameter distribution curve of the variogram at a water content of 100%: (a) contour map, (b) 3D map, (c) sill, and (d) range (red arrow represents the direction along the x-axis and the position of the load surface).

shear direction, but the fracture face is relatively flat along the vertical direction of the shear (Figures 6(a) and 6(b)). Correspondingly, the maximum sill is along the shear direction and the maximum of range is perpendicular to the shear direction (Figures 6(c) and 6(d)). Therefore, it follows that the sill represents the height of the fluctuation body in a fracture surface and the range represents the single fluctuation body and can reflect the frequency of fluctuation.

4. Discussion

The morphology of the fracture surface not only reflects the failure process [37] but also plays a dominant role in the mechanical and hydraulic behavior of discontinuous rock masses. In the literature, the morphology of the fracture surface was measured based mainly on 2D and 3D parameters. The 2D parameters are mainly concentrated in the JRC proposed by Barton and Choubey [43]. The 3D parameters are mainly concentrated in the fractal dimension [44–46]. However, the 2D parameters are limited by excessive data [47], while the 3D parameters are limited by poor directionality [48]. Wang et al. [39] proposed that based on the morphology of sheared fracture surfaces, the process of crack initiation and propagation during shear failures can be obtained and pointed that two parameters (C and a) in the variogram were effectively to quantify the anisotropy of fracture surfaces: the sill (C) can reflect the height of the fluctuation body in the fracture surface and the range (a) can reflect the single fluctuation body and its fluctuation frequency.

To quantify the anisotropy of the shear fracture surface, the anisotropic coefficient (ξ) was adopted [49], which is defined as the ratio of physical and mechanical parameters in the weakest direction to those in the strongest direction. Curves of the parameters of the variogram function of the shear fracture surface under different water contents are shown in Figure 7. It can be seen that both the maximum values of the sill and range parameters change with the same trend, decreasing when the water content was 50% and increasing when the water was 100% (see Figures 7(a) and 7(b)). This was due to the fact that the sample had a uniform internal stress distribution under dry or saturated conditions and the crack propagation path was consistent with the stress direction. However, when the water content was 50%, under compression-shear stress, the water in the sample penetrated

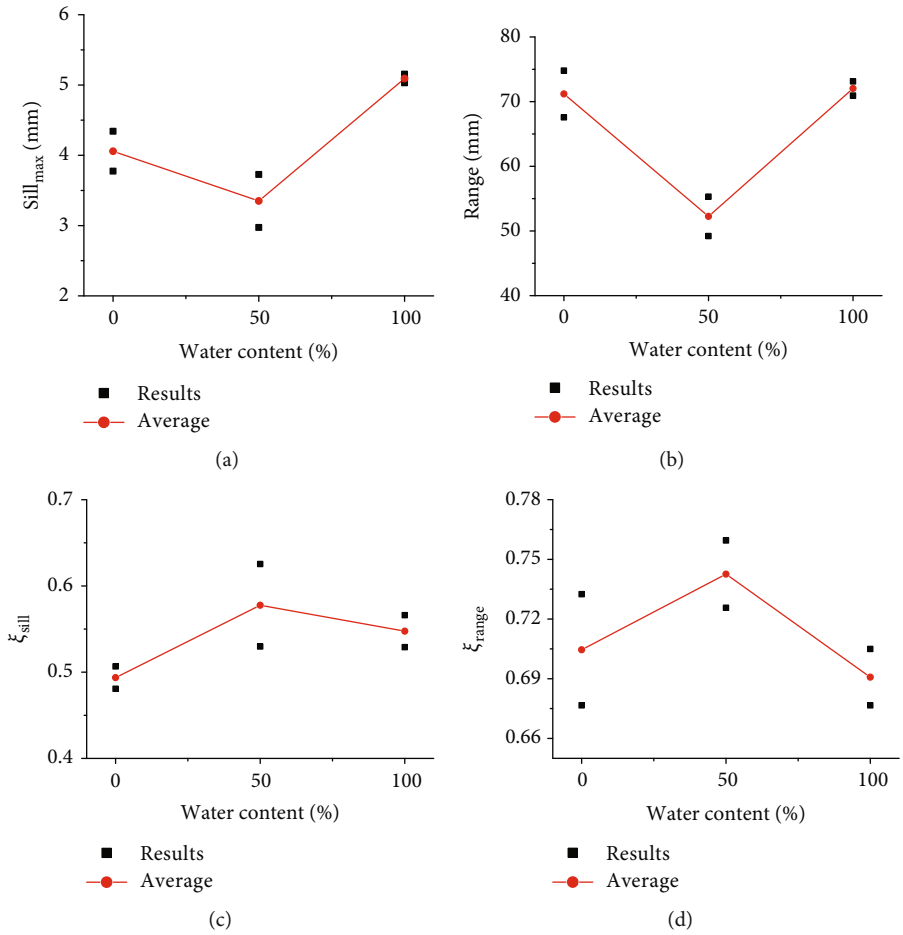

FIGURE 7: Curves of the parameters of the variogram function of the shear fracture surface under different water contents: (a) sill$_{max}$, (b) range$_{max}$, (c) ξ_{sill}, and (d) ξ_{range}.

from the interior into the surrounding area. Due to restriction of the seepage channels, the water content is too high, or a higher pore water pressure is generated locally, which results in an uneven distribution of the stress field inside the sample. In consequence, crack propagation at the center of the sample is more complicated than that in the surrounding area and leads to a decrease in the maximum values of sill and range. Similarly, when the water content was 0% and 100% (see Figures 7(c) and 7(d)), the directionality of the shear fracture surface parameters was more evident, resulting in a reduction in the anisotropy coefficient (ξ_{sill} and ξ_{range}) and more obvious anisotropy characteristics.

5. Conclusions

The morphology of a fracture surface not only reflects the failure process but also plays a dominant role in the mechanical and hydraulic behavior of discontinuous rock masses. In the present investigation, direct shear tests were carried out on sandstone to investigate the effect of water content on the shear failure mechanism of the rock and the anisotropy characteristics of the shear fracture surface. The morphology of the surface was digitized using a 3D scanner, and the anisotropy of the shear fracture surface was calculated by employing the variogram. The following conclusions were obtained:

(1) According to the results of the present study, the increase in water content has a significant weakening effect on the shear strength and deformation of rock. When the water content is increased to 50%, the shear stress was decreased by about 6%. However, when the water content reaches 100%, the peak shear stress decreased by 20%

(2) The weakening effect of water on the mechanical properties of rock included physical chemistry changes (exfoliation, hydration, solution, oxidation, and abrasion) and mechanical action (due to pore pressure). The effect of mechanical action on shear strength was greater

(3) It is reasonable that the variogram can be applied to describe the anisotropic characteristics of the shear fracture surface. When the sample was in an unsaturated state, the water content will redistribute under external load, which directly affects the crack propagation path and hence the morphology of the fracture surface

(4) The relationship between the weakening effect of the water content on the mechanical properties of the rock and its fracture surface morphology was inconsistent. However, both the mechanical properties and fracture surface morphology are related to the microcracking mechanism

Data Availability

The data used to support the findings of this study are available from the corresponding author upon request.

Conflicts of Interest

The authors declare that they have no conflicts of interest.

Acknowledgments

This research was funded by the National Natural Science Foundation of China (grant number 51704187); Shandong Province Key Research and Development Plan, China (grant number 2019GSF109068); Shandong Natural Science Foundation, China (grant numbers ZR2017BEE054 and ZR2019QEE029); Postdoctoral Innovation Project of Shandong Province, China (grant number 201703024); and Postdoctoral Application Research Project of Qingdao, China (grant number 2017-267). The authors are thankful for all of the support for this basic research.

References

[1] J. Rutqvist and O. Stephansson, "The role of hydromechanical coupling in fractured rock engineering," *Hydrogeology Journal*, vol. 11, no. 1, pp. 7–40, 2003.

[2] N. Zhang, F. Zhao, P. Guo et al., "Nanoscale pore structure characterization and permeability of mudrocks and fine-grained sandstones in coal reservoirs by scanning electron microscopy, mercury intrusion porosimetry, and low-field nuclear magnetic resonance," *Geofluids*, vol. 2018, Article ID 2905141, 20 pages, 2018.

[3] G. Wang, Y. Liu, and J. Xu, "Short-term failure mechanism triggered by hydraulic fracturing," *Energy Science & Engineering*, pp. 1–10, 2019.

[4] S. C. Yuan and J. P. Harrison, "Development of a hydro-mechanical local degradation approach and its application to modelling fluid flow during progressive fracturing of heterogeneous rocks," *International Journal of Rock Mechanics and Mining Sciences*, vol. 42, no. 7-8, pp. 961–984, 2005.

[5] H. Riegel, M. Zambrano, F. Balsamo, L. Mattioni, and E. Tondi, "Petrophysical properties and microstructural analysis of faulted heterolithic packages: a case study from Miocene turbidite successions, Italy," *Geofluids*, vol. 2019, Article ID 9582359, 23 pages, 2019.

[6] X. S. Tang, D. Q. Li, X. G. Wang, and K. K. Phoon, "Statistical characterization of shear strength parameters of rock mass for hydropower projects in china," *Engineering Geology*, vol. 245, pp. 258–265, 2018.

[7] L. Yu, R. Liu, and Y. Jiang, "A review of critical conditions for the onset of nonlinear fluid flow in rock fractures," *Geofluids*, vol. 2017, Article ID 2176932, 17 pages, 2017.

[8] S.-P. Li, D.-X. Wu, W.-H. Xie et al., "Effect of confining presurre, pore pressure and specimen dimension on permeability of Yinzhuang Sandstone," *International Journal of Rock Mechanics and Mining Sciences*, vol. 34, no. 3-4, pp. 175.e1–175.e11, 1997.

[9] J. Liu, D. Elsworth, B. H. Brady, and H. B. Muhlhaus, "Strain-dependent fluid flow defined through rock mass classification schemes," *Rock Mechanics and Rock Engineering*, vol. 33, no. 2, pp. 75–92, 2000.

[10] C. A. Tang, L. G. Tham, P. K. K. Lee, T. H. Yang, and L. C. Li, "Coupled analysis of flow, stress and damage (fsd) in rock failure," *International Journal of Rock Mechanics and Mining Sciences*, vol. 39, no. 4, pp. 477–489, 2002.

[11] Y. X. Xiao, C. F. Lee, and S. J. Wang, "Assessment of an equivalent porous medium for coupled stress and fluid flow in fractured rock," *International Journal of Rock Mechanics and Mining Sciences*, vol. 36, no. 7, pp. 871–881, 1999.

[12] J. Heiland and S. Raab, "Experimental investigation of the influence of differential stress on permeability of a lower Permian (rotliegend) sandstone deformed in the brittle deformation field," *Physics and Chemistry of The Earth Part A-Solid Earth and Geodesy*, vol. 26, no. 1-2, pp. 33–38, 2001.

[13] S. Y. Wang, S. W. Sloan, S. G. Fityus, D. V. Griffiths, and C. A. Tang, "Numerical modeling of pore pressure influence on fracture evolution in brittle heterogeneous rocks," *Rock Mechanics and Rock Engineering*, vol. 46, no. 5, pp. 1165–1182, 2013.

[14] J. Geertsma, "Some rock-mechanical aspects of oil and gas well completions," *Society of Petroleum Engineers Journal*, vol. 25, no. 6, pp. 848–856, 1985.

[15] M. El Hariri, R. E. Abercrombie, C. A. Rowe, and A. F. do Nascimento, "The role of fluids in triggering earthquakes: observations from reservoir induced seismicity in Brazil," *Geophysical Journal International*, vol. 181, no. 3, pp. 1566–1574, 2010.

[16] M. E. French and W. Zhu, "Slow fault propagation in serpentinite under conditions of high pore fluid pressure," *Earth and Planetary Science Letters*, vol. 473, pp. 131–140, 2017.

[17] S. Murphy, G. S. O'Brien, J. McCloskey, C. J. Bean, and S. Nalbant, "Modelling fluid induced seismicity on a nearby active fault," *Geophysical Journal International*, vol. 194, no. 3, pp. 1613–1624, 2013.

[18] J. Charléty, N. Cuenot, L. Dorbath, C. Dorbath, H. Haessler, and M. Frogneux, "Large earthquakes during hydraulic stimulations at the geothermal site of Soultz-sous-Forets," *International Journal of Rock Mechanics and Mining Sciences*, vol. 44, no. 8, pp. 1091–1105, 2007.

[19] Y. Guglielmi, F. Cappa, J. P. Avouac, P. Henry, and D. Elsworth, "Seismicity triggered by fluid injection-induced aseismic slip," *Science*, vol. 348, no. 6240, pp. 1224–1226, 2015.

[20] K. Hashiba, K. Fukui, M. Kataoka, and S. Y. Chu, "Effect of water on the strength and creep lifetime of andesite," *International Journal of Rock Mechanics and Mining Sciences*, vol. 108, pp. 37–42, 2018.

[21] M. Cai and D. Liu, "Study of failure mechanisms of rock under compressive-shear loading using real-time laser holography," *International Journal of Rock Mechanics and Mining Sciences*, vol. 46, no. 1, pp. 59–68, 2009.

[22] A. Kotousov, L. Bortolan Neto, and S. S. Rahman, "Theoretical model for roughness induced opening of cracks subjected to compression and shear loading," *International Journal of Fracture*, vol. 172, no. 1, pp. 9–18, 2011.

[23] W. Gao, S. Dai, T. Xiao, and T. He, "Failure process of rock slopes with cracks based on the fracture mechanics method," *Engineering Geology*, vol. 231, pp. 190–199, 2017.

[24] X. G. Liu, W. C. Zhu, Q. L. Yu, S. J. Chen, and R. F. Li, "Estimation of the joint roughness coefficient of rock joints by consideration of two-order asperity and its application in double-joint shear tests," *Engineering Geology*, vol. 220, pp. 243–255, 2017.

[25] L. Ban, C. Qi, and C. Lu, "A direction-dependent shear strength criterion for rock joints with two new roughness parameters," *Arabian Journal of Geosciences*, vol. 11, no. 16, 2018.

[26] H. K. Singh and A. Basu, "Evaluation of existing criteria in estimating shear strength of natural rock discontinuities," *Engineering Geology*, vol. 232, pp. 171–181, 2018.

[27] T. Xu, Q. Xu, C. A. Tang, and P. G. Ranjith, "The evolution of rock failure with discontinuities due to shear creep," *Acta Geotechnica*, vol. 8, no. 6, pp. 567–581, 2013.

[28] Y. Liu, J. Xu, G. Yin, and S. Peng, "Development of a new direct shear testing device for investigating rock failure," *Rock Mechanics and Rock Engineering*, vol. 50, no. 3, pp. 647–651, 2017.

[29] Y. Liu, J. Xu, and G. Zhou, "Relation between crack propagation and internal damage in sandstone during shear failure," *Journal of Geophysics and Engineering*, vol. 15, no. 5, pp. 2104–2109, 2018.

[30] Z. Zhou, X. Cai, W. Cao, X. Li, and C. Xiong, "Influence of water content on mechanical properties of rock in both saturation and drying processes," *Rock Mechanics and Rock Engineering*, vol. 49, no. 8, pp. 3009–3025, 2016.

[31] N. Babanouri and S. Karimi Nasab, "Modeling spatial structure of rock fracture surfaces before and after shear test: a method for estimating morphology of damaged zones," *Rock Mechanics and Rock Engineering*, vol. 48, no. 3, pp. 1051–1065, 2015.

[32] G. Grasselli, "Shear strength of rock joints based on quantified surface description," No. THESIS. EPFL, 2004.

[33] P. Baud, W. Zhu, and T. F. Wong, "Failure mode and weakening effect of water on sandstone," *Journal of Geophysical Research: Solid Earth*, vol. 105, no. B7, pp. 16371–16389, 2000.

[34] J. Xu, Y. Liu, and S. Peng, "Acoustic emission parameters of three gorges sandstone during shear failure," *Acta Geophysica*, vol. 64, no. 6, pp. 2410–2429, 2016.

[35] V. Gupta and I. Ahmed, "The effect of pH of water and mineralogical properties on the slake durability (degradability) of different rocks from the lesser Himalaya, India," *Engineering Geology*, vol. 95, no. 3-4, pp. 79–87, 2007.

[36] F. M. Aben, M. L. Doan, J. P. Gratier, and F. Renard, "High strain rate deformation of porous sandstone and the asymmetry of earthquake damage in shallow fault zones," *Earth and Planetary Science Letters*, vol. 463, pp. 81–91, 2017.

[37] K. Takahashi, M. Kido, and K. Arakawa, "Fracture roughness evolution during mode I dynamic crack propagation in brittle materials," *International journal of fracture*, vol. 90, no. 1/2, pp. 119–131, 1998.

[38] H. W. Zhou and H. Xie, "Anisotropic characterization of rock fracture surfaces subjected to profile analysis," *Physics Letters A*, vol. 325, no. 5-6, pp. 355–362, 2004.

[39] G. Wang, Y. Liu, and J. Xu, "Anisotropic characteristics of post sheared fracture surface," *International Journal of Geomechanics*, 2019.

[40] A. Marache, J. Riss, S. Gentier, and J. P. Chilès, "Characterization and reconstruction of a rock fracture surface by geostatistics," *International Journal for Numerical and Analytical Methods in Geomechanics*, vol. 26, no. 9, pp. 873–896, 2002.

[41] T. Suzuki, M. Aoki, and M. Ohtsu, *Damage quantification of concrete surface layers by semi-variogram analysis*, ICF12 Ottawa, 2009.

[42] B. T. Brady, "A statistical theory of brittle fracture for rock materials part I–brittle failure under homogeneous axisymmetric states of stress," *International Journal of Rock Mechanics and Mining Sciences & Geomechanics Abstracts*, vol. 6, no. 1, pp. 21–42, 1969.

[43] N. Barton and V. Choubey, "The shear strength of rock joints in theory and practice," *Rock Mechanics and Rock Engineering*, vol. 10, no. 1-2, pp. 1–54, 1977.

[44] N. E. Odling, "Natural fracture profiles, fractal dimension and joint roughness coefficients," *Rock Mechanics and Rock Engineering*, vol. 27, no. 3, pp. 135–153, 1994.

[45] P. H. S. W. Kulatilake and J. Um, "Requirements for accurate quantification of self-affine roughness using the roughness-length method," *International Journal of Rock Mechanics and Mining Sciences*, vol. 36, no. 1, pp. 5–18, 1999.

[46] T. Koyama, N. Fardin, L. Jing, and O. Stephansson, "Numerical simulation of shear-induced flow anisotropy and scale-dependent aperture and transmissivity evolution of rock fracture replicas," *International Journal of Rock Mechanics and Mining Sciences*, vol. 43, no. 1, pp. 89–106, 2006.

[47] Z. Y. Yang and S. C. Lo, "An index for describing the anisotropy of joint surfaces," *International Journal of Rock Mechanics and Mining Sciences*, vol. 34, no. 6, pp. 1031–1044, 1997.

[48] N. Fardin, O. Stephansson, and L. R. Jing, "The scale dependence of rock joint surface roughness," *International Journal of Rock Mechanics and Mining Sciences*, vol. 38, no. 5, pp. 659–669, 2001.

[49] J. Feder, *Fractals*, Springer US, 1988.